keV particle bombardment of semiconductors: A molecular-dynamics simulation

Roger Smith* and Don E. Harrison, Jr.†
Department of Physics, Naval Postgraduate School, Monterey, California 93943

Barbara J. Garrison
Department of Chemistry, The Pennsylvania State University, University Park, Pennsylvania 16802
(Received 27 February 1989)

Molecular-dynamics simulations have been performed for the keV particle bombardment of Si{110} and Si{100} using a many-body potential developed by Tersoff. Energy and angle distributions are presented along with an analysis of the important ejection mechanisms. We have developed a computer logic that only integrates the equations of motion of the atoms that are struck, thus decreasing the computer time by a factor of 3 from a complete molecular-dynamics simulation.

I. INTRODUCTION

The keV particle bombardment of solids is a technique used for fabrication of devices in the semiconductor industry, for mass measurements of biological compounds and for structural determinations of surface bonding arrangements. Although the process may seem quite complex due to the large number of atomic and molecular motions involved, molecular-dynamics computer simulations have been quite successful at predicting experimental observables and explaining microscopic mechanisms of ejection such as how large molecules adsorbed on the surface eject intact.[1,2] One of the successes of the molecular-dynamics simulations is that it can quantitatively predict the energy and angular distributions of the particles that eject from the surface.[3–9] The main concept that has arisen from the simulations is that channeling and blocking by neighboring atoms dominate the angular distributions. Surface channeling facilitates ejection of atoms along open azimuthal surface directions and inhibits the ejection along close-packed azimuths. The molecular-dynamics simulations along with experimentally measured angular distributions have been used to determine structures of clean[6–8] and adsorbate-covered[4,9,10] metal surfaces. There are indications,[11–14] however, that the important collision mechanisms may be quite different for semiconductors where the substrate is more open. That is, if one assumes a solid to be composed of spheres where nearest-neighbor atoms touch, the diamond lattice structure of silicon is 34% occupied and 68% open space.[15] In contrast a face-centered-cubic material is 74% occupied and only 26% open space. Preliminary angle-resolved secondary ion mass spectrometry (SIMS) (Ref. 13) and multiphoton resonance ionization (MPRI) energy- and angle-resolved neutral (EARN) data[14] on GaAs {110} (Fig. 1) show quite striking angular distributions which are unexplainable if, as for metals, the channeling and blocking by surface neighbor atoms dominate the ejection process. In addition, on the unreconstructed Si {100} face (Fig. 1), the "open" direction is along the azimuthal directions of $\varphi=0°,90°,\ldots$ of Fig. 1, but Stansfield *et al.*[12] in molecular-dynamics simulations and MacDonald in experiments[11] find that the preferred ejection is along $\varphi=45°,135°,\ldots$.

The use of molecular dynamics calculations to model the keV particle bombardment of solids is quite widespread, although the majority of the work has been

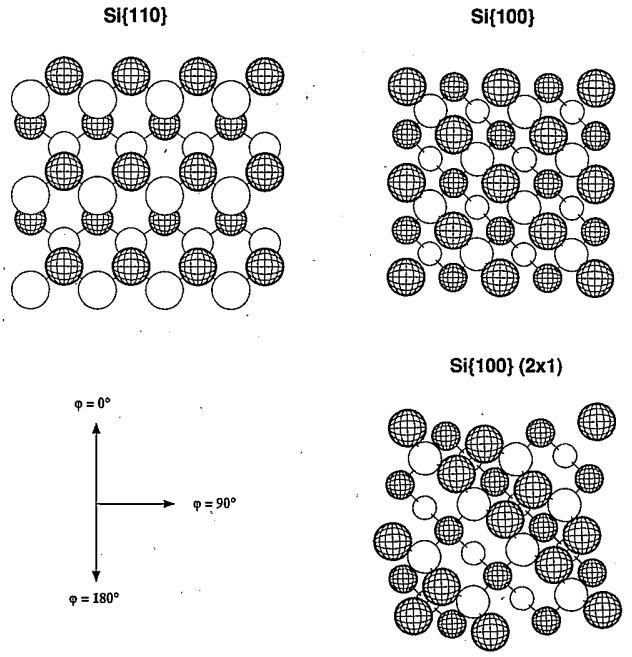

FIG. 1. Silicon surface arrangements. For Si{110}, the larger circles represent top layer atoms and the smaller circles represent second layer atoms. The third layer is directly below the first layer. The hatched circles (Si_h) would be Ga atoms in a GaAs{110} surface, and the open circles (Si_o) would be As atoms. For Si{100}, four layers are exposed with largest circles representing the top layer atoms and the smallest circles the fourth layer atoms. The hatching is for artistic purposes only, although it too represents the GaAs crystal arrangement. For Si{100} (2×1), the same orientation and notation is used here as for the Si{100} bulk terminated surface. The azimuthal angles, φ, as used in the text are also described.

performed on metals. This is primarily because the interaction potentials necessary to accurately describe the bonding in open crystals structures such as silicon have just recently been developed.[16–24] At this stage, a number of Si potentials are in the literature, and the time is ripe for examining the details of the ejection mechanisms for open crystal structures and the influence of the atomic motions on the angular distributions.

In this paper, we present the results of molecular dynamics calculations of Ar bombardment of Si {110}, bulk terminated Si {100}, and the dimer reconstructed Si{100} (2×1) (Ref. 25) faces using the Tersoff potential[20] for the attractive interactions among the Si atoms and Molière potentials for the very short-range repulsive interactions. These results will be compared to the molecular dynamics study of Stansfield *et al.* for Si{100} (Ref. 12). In addition to examining the mechanisms of ejection in open crystals, we show that the computer time required for the molecular dynamics calculations can be significantly decreased by using a moving atom approximation.[26] In this case, the equations of motion of only atoms that are moving or have had a sufficient force exerted on them by other atoms are integrated in time. This is a significant time saving feature for open crystals, as there are numerous trajectories where the Ar particle or one of the Si atoms finds a channel and moves through the solid without strongly interacting with any other atoms.

We find that although there is channeling and blocking of the ejecting atoms by surface atoms, a number of other mechanisms also contribute to the ejection of Si atoms from the open lattice. For example, the yields have relatively large components from second and third layer atoms, whereas for low index faces of metals, primarily only the first layer atoms are found to eject.[27] The angular distributions cannot be predicted from the surface channeling and blocking arguments developed for metal surfaces. Although the angular distributions, especially those from the {100} faces, appear to be dominated by direct neighbor-neighbor collisions, the collision mechanisms that lead to ejection are quite complex. The peaks in the calculated energy distributions are higher than one would predict from simple transport theories.[28–31]

The description of the moving atom approximation and the interaction potential are given in Sec. II. The results with an emphasis on the angular distributions is given in Sec. III, followed by the conclusions in Sec. IV.

II. DESCRIPTION OF THE CALCULATION

A classical dynamics prescription is used to model the motion in the substrate subsequent to the keV particle bombardment. A microcrystallite of atoms approximates the single-crystal substrate. The primary particle, whose energy and angle of incidence are known, is aimed at the surface. The motion of all the atoms is then determined by integrating Newton's equation of motion cast as coupled first-order differential equations. The final momenta and positions of the ejected species are used to calculate the energy and angular distributions of the silicon atoms. In addition, the microscopic mechanisms of ejection can be determined by following the atomic motions. A complete description of the calculational procedure has been given elsewhere.[26,32]

The two main unique aspects of this calculation are the potential and the moving atom logic. There are a multitude of many-body potentials that have recently been developed for bulk silicon.[16–24] We have chosen to use the potential of Tersoff,[20] as his potentials are fit not only to the diamond lattice strucutre, but also to overcoordinated and undercoordinated configurations. Aesthetically, this is attractive, as it leaves open the possibility of examining defect structures and processes such as molecular-beam epitaxy (MBE) of silicon.[33–35] The second of Tersoff's potentials[20] was chosen, as it was the most refined when these calculations were initiated; however, the third[21] appears better for surface reactions such as MBE (Ref. 35).

Tersoff writes the total energy as

$$E=\frac{1}{2}\sum_{i\neq j}[V_R(r_{ij})+B_{ij}V_A(r_{ij})]\ ,$$

where r_{ij} is the distance between atoms i and j, V_R is a repulsive term, V_A is an attractive term, and B_{ij} is a many-body term that depends on the positions of atoms i and j and the neighbors of atom i. It should be pointed out that B_{ij} is *not* invariant in the interchange of labels i and j, and it is this term that incorporates the many-body features of the potential. The term V_R is rigorously a two-body term. The nature of B_{ij} and all the parameters have been defined by Tersoff.[20] Unfortunately, this potential is not sufficiently repulsive at short internuclear separations to be used in simulations of keV particle bombardment. To incorporate a more repulsive Si-Si interaction, we have connected the repulsive pair part V_R to a Molière potential with a screening length of 0.83 times the Firsov value.[36] We have developed a procedure that gives a smoother connection of both the interaction potential and the force than just a straight spline at distances of r_a and r_b, 0.358 Å and 0.543 Å, respectively, in this case. A function of the form $V_{\rm fit}=\exp(ar+b)$ with a and b constants, is fit to the *forces* of the Molière at r_a and V_R at r_b. The forces are now defined derivatives of the Molière potential at distances less than r_a, of V_R for distances greater than r_b, and of $V_{\rm fit}$ for the intermediate range. The interaction potential is determined for distances less than r_b by integrating $V_{\rm fit}$ from r_b to r_a. At r_a the Molière potential is shifted to ensure continuity. This procedure gives the overall smoothest fit, although the resulting Molière potential is shifted somewhat. At the distance $r_a=0.358$ Å the overall repulsive potential is about 1200 eV, in this case above the collision energies used. The Molière potential was shifted upward by 122.6 eV. However, to get the total two-body potential, the attractive potential V_A must be included which then shifts the potential downward by 61.9 eV. The overall shift at r_a is about 5% of the Molière potential that was originally assumed. For the Ar-Si interaction, we have used a Molière potential with a screening length of 0.80 times the Firsov value. The Ar-Si potential has a cutoff distance of 3.4 Å.

Molecular dynamics calculations are relatively lengthy, especially when a many-body interaction potential and 1000–2000 atoms are used. In an effort to make the calculations more efficient, we have investigated a moving atom approximation for the simulations.[26] Instead of calculating the forces for *all* the atoms, we only integrate the equations of motion for the *moving* atoms. Initially the only moving particle is the Ar atom. The forces among the Ar atom and its Si neighbors (within the cutoff distance of the potential) are evaluated. All of these forces are exerted on the Ar atom and influence its subsequent motion. If the force on any one Si atom is less than a given threshold, then the force is assumed to be zero and this atom's position is not altered. If the force is greater than this specified value, then the atom is "turned on," all the forces on it are evaluated, and its equations of motion are integrated. This process is repeated at each step with more and more atoms being turned on. The energy conservation during the integration is checked for each value of the turn-on force threshold in order to ascertain that severe approximations are not being made. We feel that this type of approximation is particularly appropriate for simulations of particle bombardment, as the total ejection process occurs in less than 0.5×10^{-12} s. Only the motions of the atoms due to collisions are important on this time scale. Thermal motions due to small forces are relatively unimportant. Another factor that makes the moving atom approximation attractive in this case is the presence of open channels in the Si crystal.

The moving atom approximation must be treated with caution and tested carefully for each type of simulation, as when it breaks down the errors are systematic. As the force threshold assumed in the calculation is increased, the energy is more slowly dispersed in the solid. A moving atom, if it cannot transfer energy to its neighbors, retains extra energy. Some atoms, therefore, artifically have too much energy, and escape from the solid. The resulting ejection yields are too large and the energy distribution peaks at too small a value.

The crystal sizes for the simulations presented here are 210 atoms in 7 layers for the Si{110} surface, 155 atoms in 11 layers for the Si{100} surface, and 128 atoms in 10 layers for the dimer reconstructed[25] Si{100} (2×1) surface. Portions of each face are shown in Fig. 1. The crystal sizes in angstrom units are approximately equal. For Si{110} and Si{100}, the bulk terminated positions were assumed for the surface atoms. The atom positions for the Si{100} (2×1) surface were determined by a molecular dynamics simulation with periodic boundary conditions in the two horizontal directions.[35] The binding energy of the top layer silicon atoms is 3.92 eV for the {110} and {100} (2×1) surfaces. The energy of an atom in the top layer of the {100} face is 2.62 eV. These energies are approximately proportional to the number of first neighbor atoms that the surface atom has, even though the Tersoff potential is many-body in nature.

In the case of the {110} face, energies of the Ar particle are chosen between 100 and 1000 eV. For the two {100} faces, only trajectories at 1000 eV are calculated. In all cases, the Ar particle is aimed in the direction normal, i.e., perpendicular, to the surface. The final velocities of the ejecting species are used to calculate the energy and angular distributions.

III. RESULTS AND DISCUSSION

The molecular dynamics simulations show clearly that the nature of the ejection process and the experimental observables such as energy and angular distributions are dominated by the openness of the silicon crystal. In contrast to the silicon crystal surfaces shown in Fig. 1, if one were to draw a low Miller index plane of a face-centered-cubic crystal, for the most part, only the first layer atoms would be visible. For Si{100}, four layers are clearly seen from the perspective of the primary particle and for Si{110}, two layers are visible along with some large open channels. This openness means that the Ar or one of the initially struck Si atoms can penetrate a relatively long distance in the crystal. In view of an atom escaping the solid, there are also channels into which it can move and easily escape.

The first reflection of the openness of the crystal is shown in Tables I and II. For Ar bombardment at 1000 eV, the yield (average number of Si atoms ejected per incident Ar particle) of the more open {110} face is less than for the {100} faces. Correspondingly, the computer time for the {110} face is about one-third that for the {100} faces. There are *many* incident Ar particles on {110} that travel straight through the crystal and require less than 1 s of CPU time (Table I). There are many fewer of these instantaneous trajectories on the {100} faces. As shown in Table II, there are a multitude of atoms that eject from the second and third layers since there are open channels that allow them to escape easily. For simulations on low index faces of metals at comparable Ar energies, one finds that there are relatively few very short Ar trajectories, and that 90–95% of the atoms eject from the first layer.[27] All of the incident Ar atoms in the simulations presented here were found to implant on all faces.

The moving atom approximation was tested by comparing the yields and energy distributions of calculated results to those performed without this approximation using 1000 eV Ar bombardment of Si{110}. As shown in Table I, for the same 300 Ar impacts on the surface, the yield using a force threshold of 1.12×10^{-9} N is 5% higher than without using the approximation. If the threshold is increased by a factor of 2.5 (2.8×10^{-9} N), then the yield is 15% too high. Of note is that the computer time does not decrease continuously with an increase in the force threshold. As the threshold gets higher, fewer and fewer atoms are moving and it takes longer for the energy to dissipate in the crystal. That is, each integration step may be shorter, but more steps must be taken before the collision cascade is finished. Shown in Fig. 2(a) are the energy distributions for each of the force thresholds. For the threshold value of 2.8×10^{-9} N, the distribution peaks at 1–2 eV *below* the distributions with lower thresholds. As stated above, this peak shift and the increased yields are *systematic* errors. A set of our snapshots where atoms are "turned-on" during one Ar impact is shown in Fig. 3. *It is readily ap-*

TABLE I. Calculated number of particles that eject as a function of energy in eV using the moving atom approximation with a force threshold of 1.12×10^{-9} N.

Face	Energy (eV)	No. Ar impacts	No. Si ejected	Yield	CPU time[a]
{110}	100	300	10	0.03	25
{110}	200	300	31	0.10	45
{110}	400	300	65	0.22	58
{110}	600	300	104	0.35	65
{110}	800	300	122	0.41	66
{110}	1000	5400	2306	0.43	68
{110}	1000	300	133[b]		225
{110}	1000	300	139[c]		68
{110}	1000	300	153[d]		67
{100}	1000	2700	2929	1.08	152
{100} (2×1)	1000	2700	1774	0.66	117

[a]Average time per Ar impact in seconds on an IBM 3090/400E using FORTVS2 (opt=2).
[b]Force threshold of zero.
[c]Same 300 Ar impacts as with the force threshold of zero except that the threshold is 1.12×10^{-9} N.
[d]Same 300 Ar impacts as with the force threshold of zero except that the threshold is 2.80×10^{-9} N.

parent that at the beginning of the collision cascade there are many atoms which feel no effect of the Ar impact, and it is wasteful computationally to follow their motion.

The yields are one of the easiest quantities to calculate in this molecular-dynamics approach, yet are one of the most difficult to determine accurately and to make a reasonable comparison to experimental values. As has been shown both for the ejection process of metals[27,37] and silicon,[12] the calculated yield depends on the nature of the Ar-Si repulsive wall, the Si-Si repulsive wall, the Si attractive interaction and the exposed crystal face. The experimental determinations are performed under conditions in which over the course of the measurements the same point on the surface is bombarded more than once. This means that even though the surface may have started as a pure single crystal, by the time the measurement has finished, the sample has become amorphous and contains Ar. The best we can say regarding the yields in Table I is that the {100} yields at 1000 eV are consistent with the calculated values of Stansfield *et al.*[12] and Herbots *et al.*,[38] and the experimental values of Zalm,[39] and that the {110} yields are lower than the {100} values due to the openness of the exposed crystal face.

Of more interest to this work is the influence of the open crystal structure on the angular and energy distributions of the ejected Si atoms. In many previous studies we have shown for metals that the angular distributions are useful for determining the surface structures of metals.[3,6–10] For what we believe will help clarify the angular distributions and because of experiments being performed, we have removed part of the symmetry in the distributions from the {110} surface. In the angles of Fig. 1, for Si atoms from Si{110} the azimuths $\varphi=180°$ and $\varphi=0°$ are equivalent, but for GaAs{110}, they are inequivalent. We have mapped the ejected atom distributions so that they would represent the hatched Si atoms (Si_h) of Fig. 1 distributions. This is formally the equivalent of examining the Ga atom distributions from a bulk terminated GaAs{110} surface. The angular distributions are displayed in polar form (Figs. 4–6) in which a hemispherical collector is placed around the sample. Each atom that ejects makes a point on this surface. The center of the pattern corresponds to ejection normal to the surface, i.e., $\theta=0°$, where θ is the polar angle of ejection, and the edge as grazing ejection, i.e., $\theta=90°$. These patterns provide a good overall visual impression of the angular distribution. More quantitative information is obtained from polar distributions (Fig. 7) in which the number of ejected atoms as a function of polar angle θ is plotted. To convert the spot patterns of Si_h to all Si atoms, a horizontal plane of symmetry must be included so that the top half pattern is the same as the bottom half.

TABLE II. Contribution in terms of percentage of different layers to the yield for Si{110} and Si{100}. The Ar particle had 1000 eV of kinetic energy.

Layer	Percent contribution to the yield Si{110}	Si{100}	Si{100} (2×1)
1	75%	57%	46%
2	19%	21%	31%
3	6%	20%	16%
Rest	1%	2%	7%

The patterns of Si_h atoms ejected from the Si{110} face for 1000 eV Ar bombardment are shown in Fig. 4 as a function of the Si energy and for the 15–100 eV Si atoms as a function of the layer from which the atom originated. If symmetrized with the $\varphi=0°$ and 180° directions equivalent, the overall pattern would be rectangular, as observed by MacDonald.[11] Cross sections of these spot patterns for the 15–100 eV Si atoms are displayed as

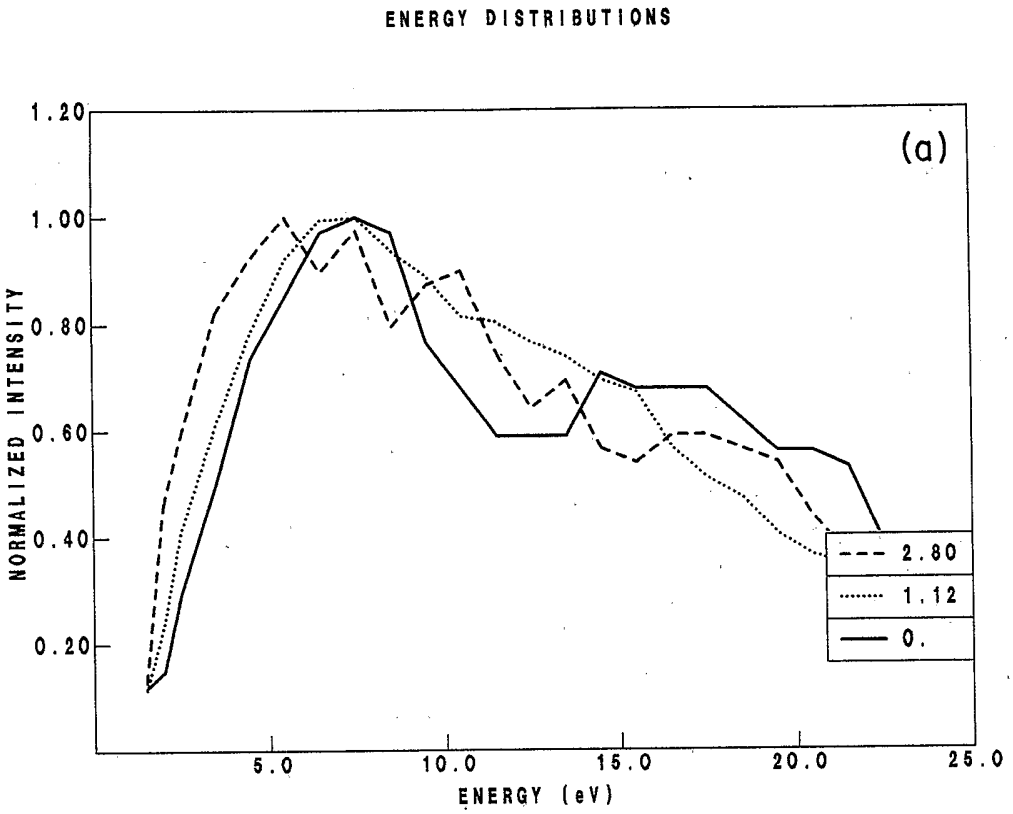

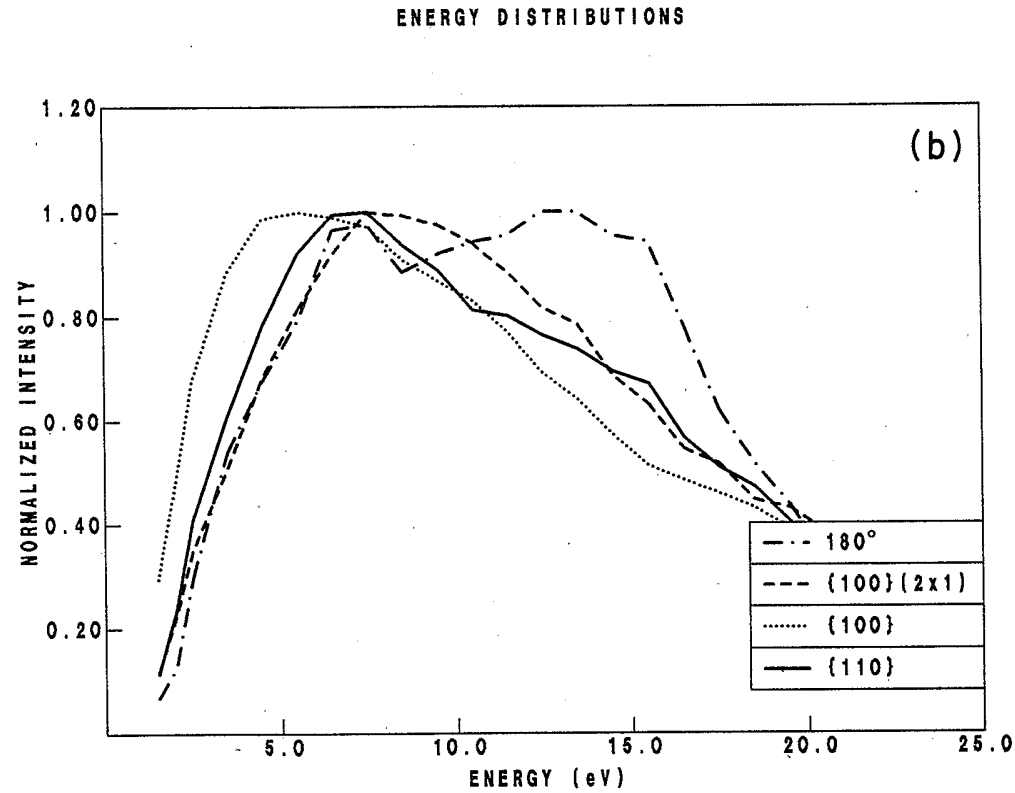

FIG. 2. Energy distributions. (a) Angle-integrated distributions from Si{110} as a function of force threshold in the moving atom approximation. The force threshold value in 10^{-9} N is given in the legend. (b) Angle-integrated distributions as a function of crystal face. The fourth curve is for Si_h atoms that eject from Si{110} at $\theta=40°\pm10°$ and $\varphi=180°$, i.e., the most intense feature of the distribution shown in Fig. 4. In all cases the Ar had 1000 eV of kinetic energy.

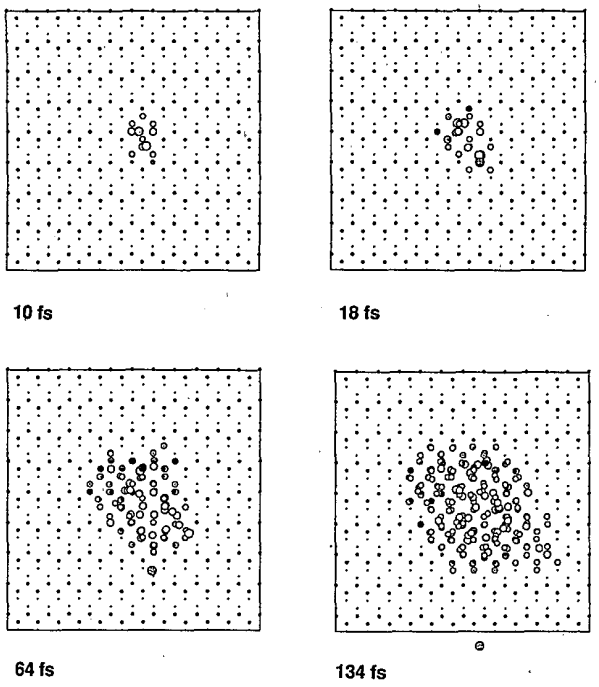

FIG. 3. Snapshots in time of the collision cascade on Si{110} using the moving atom approximation. The cascade is viewed from above the surface layer. The small dots represent the unmoving atoms. The darker of these dots represent the first layer atoms. Frames are shown at 10, 18, 64, and 134 fs (1 fs $=1\times10^{-15}$ s). The atom sizes of the moving atoms increase with increasing energy for three discrete energy ranges of <10 eV, <100 eV, and >100 eV. The atom that will ultimately eject is flagged with hatching before it ejects and a stippled pattern after it ejects. This is a collision sequence where the Ar strikes a surface Si atom. This Si atom reflects off a second layer atom and strikes another surface Si atom ejecting it along the $\varphi=180°$ azimuth.

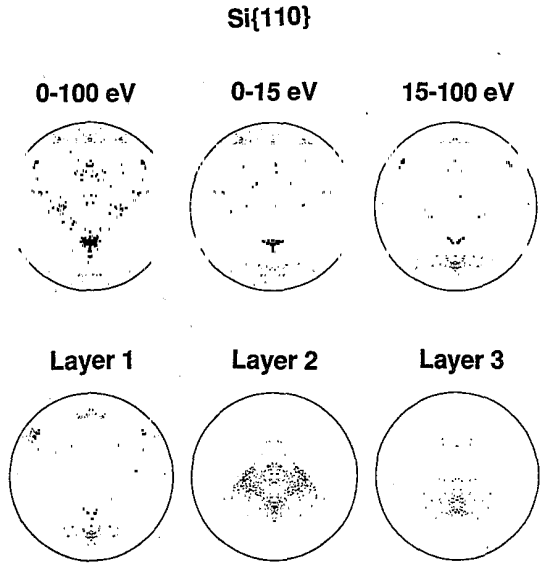

FIG. 4. Angular distributions from Si{110} for only the Si_h atoms shown in Fig. 1. The Ar has 1000 eV of kinetic energy. The top set of plots are energy selected distributions. The energy ranges from left to right are (0–100 eV), (0–15 eV), and (15–100 eV). The bottom sets of plots are for 15–100 eV particles for top layer, second layer, and third layer atoms from left to right. The total distribution of Si atoms would have a horizontal mirror plane so that each of the top and bottom halves would be a sum of the Si_h top and bottom half distributions.

polar distributions in Fig. 7. We have chosen to plot only the higher-energy particles, as it has been shown that they are more sensitive to the structure of the substrate.[3] The most intense feature occurs at $\varphi=180°$ and at a polar angle of about $\theta=40°$. This feature has contributions from atoms from all three layers. There are other peaks of note at (φ,θ) values of $(0°,40°)$, $(80°-120°,30°)$, and $(60°,75°)$.

If the concepts of surface channeling and blocking developed to explain the angular distributions from metal surfaces[3] are applied to Si{110}, then the main feature in the angular distribution should be the peak at $\varphi=180°$. Here the two surface Si_o atoms channel the ejecting Si_h atom in the 180° direction. This same channeling effect is operative for the second and third layer atoms. This channeling does in fact have an influence on the angular distributions. However, there are also direct neighbor-neighbor collisions between an Si_o atom in the second layer and a Si_h atom in the first layer, which results in the Si_h atom ejecting in the 180° direction. The same direct collisions occur for the second and third layer atoms. The small peak in Fig. 7 at $\theta=60°-65°$ and $\varphi=180°$ is due almost entirely to first layer atoms which have been

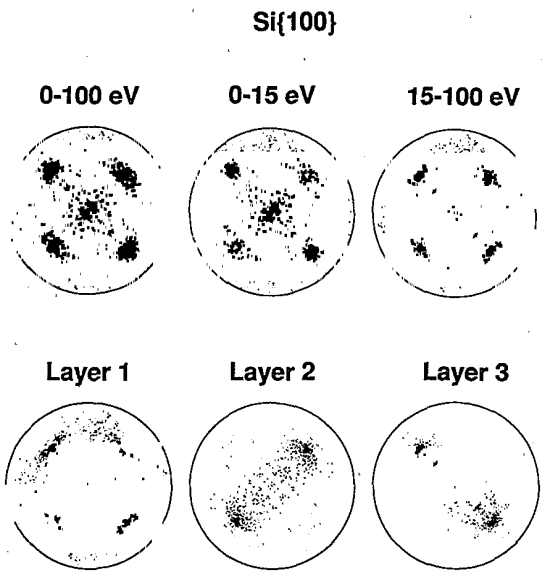

FIG. 5. Angular distributions from Si{100} oriented as shown in Fig. 1. The Ar has 1000 eV of kinetic energy. The top set of plots are energy selected distributions. The energy ranges from left to right are (0–100 eV), (0–15 eV), and (15–100 eV). The bottom set of plots are for 15–100 eV particles for top layer, second layer, and third layer atoms from left to right. The distribution along $\varphi=45°$ peaks at $\theta\approx53°$ and the distribution along $\varphi=135°$ peaks at $\theta\approx57°$.

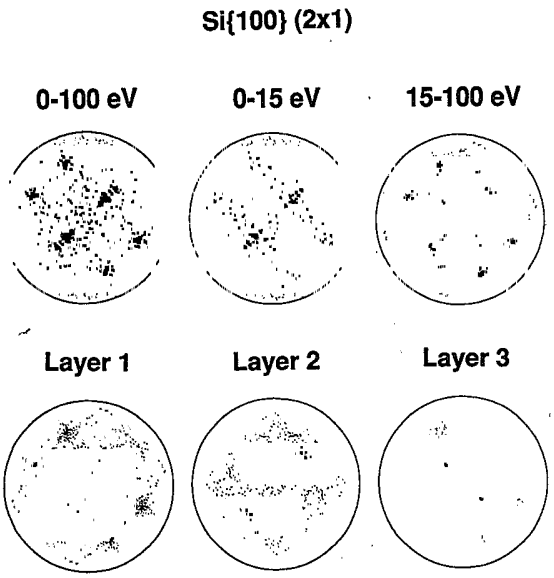

FIG. 6. Angular distributions from Si{100} (2×1) oriented as shown in Fig. 1. The Ar has 1000 eV of kinetic energy. The top set of plots are energy selected distributions. The ranges from left to right are (0–100 eV), (0–15 eV), and (15–100 eV). The bottom set of plots are 15–100 eV particles for top layer, second layer, and third layer atoms from left to right. The distribution along $\varphi=45°$ peaks at $\theta\approx40°$ and the distribution along $\varphi=113°$ peaks at $\theta\approx60°$.

hit by a second layer nearest-neighbor atom.

The openness of the crystal allows second and third layer atoms to escape. For second layer atoms they can either escape along $\varphi=180°$ as already described, or parallel to the trough in which they are bound, i.e., along $\varphi=80°-120°$. These are the only azimuths that are unblocked by the first layer atoms. Thus the peaks in these azimuths, then, have a large but not exclusive component from second layer atoms. A fraction of the atoms that try to escape along $\varphi=0°$ hit a first layer Si_h atom. Thus the peak at $\varphi=0°$ and $\theta\approx40°$ arises from collisions between first layer atoms and either second or third layer atoms that are underneath them.

The last feature is the peak at $\theta=75°$ and $\varphi=60°$. This peak is made up exclusively from one collision sequence in which the incoming Ar atom hits a Si_o atom pushing it downward and sideways towards the neighboring Si_h atom. The Si_h atom is ejected almost directly along the bond (the azimuthal direction of the Si—Si surface bond is 55°). Again a neighbor-neighbor collision is quite important. It should be pointed out that this mechanism is really the start of the alternating mechanism observed 13 years ago by Harrison,[40] but in this case, it is truncated by the lack of another neighbor atom for the Si_h atom to strike.

The analogous angular distributions for Si{100} are shown in Fig. 5. There are two almost equally intense

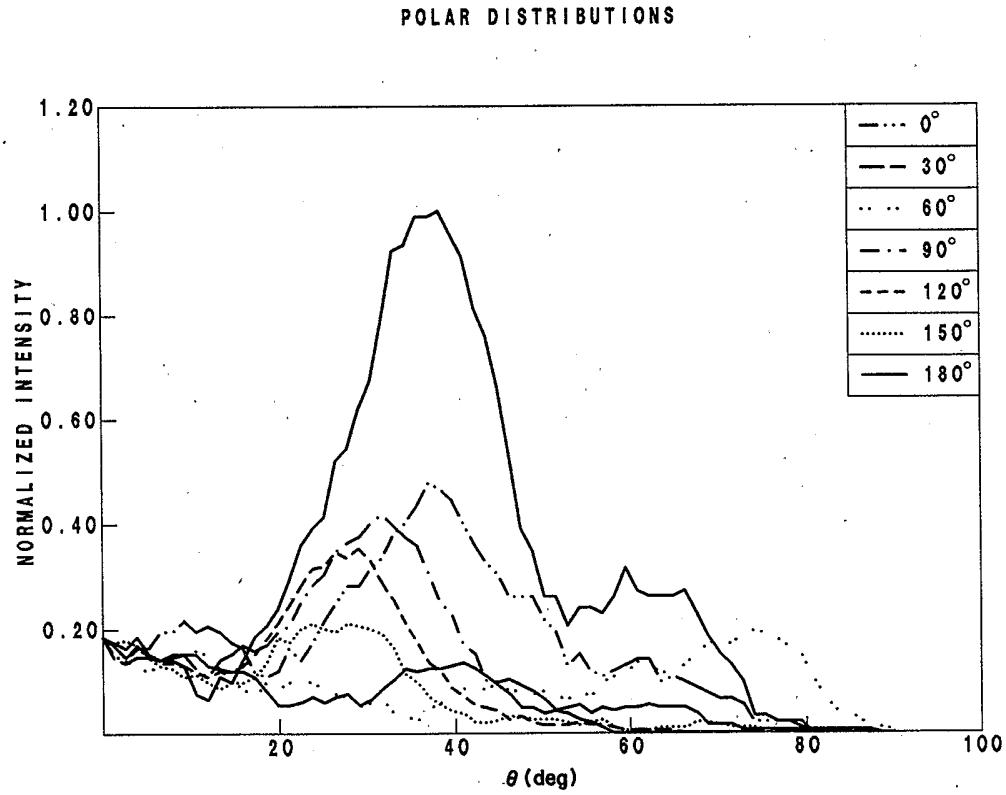

FIG. 7. Polar angle distributions for the 15–100 eV Si_h atoms for the Si{110} surface. The azimuthal angles, φ in degrees, are given in the legend. The distributions are collected with a constant solid angle of $1.7\times10^{-2}\ \pi$ sr, which is approximately a polar angle resolution of ±7.5°.

peaks in the $\varphi=45°$ and 135° directions. The first layer atoms contribute to both peaks, while the second and third layer atoms each contribute to one peak. The second layer (large Si_o atoms of Fig. 1) contribution to the spot along $\varphi=45°$ occurs in the direction of the bond from the third layer (small Si_h) atoms. Likewise, the third layer contribution to the spot along $\varphi=135°$ is oriented along the direction from the fourth layer (small Si_o) atoms. It is tempting to interpret these distributions as arising from direct neighbor-neighbor collisions. However, there are a multitude of collision processes that give rise to the ejection of atoms. What is reflected in the angular distributions is the overall symmetry and openness of the crystal. A significant number of the atoms that eject in the 15–100 eV range arise due to collisions with the Ar particle or to collisions with the first Si atom that the Ar particle struck. MacDonald in a series of experiments[11] also concluded that the direct neighbor-neighbor collisions (also called focussons) were not the dominant mechanism responsible for the peaks in the angular distributions. These effects have also been observed by Stansfield *et al.*[12] There is a small difference in peak position and intensity in the two directions with the $\varphi=45°$ distribution maximizing at $\theta\approx53°$ and the $\varphi=135°$ distribution at $\theta\approx57°$.

The angular distributions for the dimer reconstructed surface, Si{100} (2×1), are shown in Fig. 6. The crystal is oriented the same as is depicted in Fig. 1. The major change in the angular distribution from that of the bulk terminated {100} surface is in the distribution of the first layer atoms. The high intensity feature at $\varphi=45°$ almost disappears from the first layer atom distribution, and the feature at $\varphi=135°$ splits into two parts. As already stated, a multitude of collision events including collisions with the Ar particle is responsible for overall angular distributions. The major peaks in this angular distribution occur at $\varphi=45°$ and $\theta=40°$, at $\varphi=113°$ and $\theta=60°$. This distribution appears different than the one obtained by Stansfield *et al.*[12] They only plotted azimuthal angular distributions. Their distributions for Si{100} and Si{100} (2×1) were almost identical. In order to obtain an experimental verification of the predicted angular distribution, there must be a pure (2×1) structure. In the next atomic layer, the reconstruction will be (1×2) with the dimer rows at 90° to the ones shown in Fig. 1. If both reconstructions are present, the angular distribution will be a linear combination of that shown in Fig. 6 along with one rotated by 90°.

The kinetic energy distributions for the three crystal faces are shown in Fig. 2(b). The angle-integrated distribution from Si{110} peaks at about 7 eV, the one from Si{100} at about 5 eV, and the one from Si{100} (2×1) at 8 eV. Transport theories of sputtering[28–31] predict that the peak position should occur at a value proportional to the energy cost to remove an atom. For metals, the peak in the energy distributions occurs in the range of 0.5–0.8 times the heat of sublimation or cohesive energy.[30] The cohesive energy of Si is 4.63 eV.[41] The energy value of the peak position in our case is *greater* than the cohesive energy. We believe that this is ascribable to the fact that there are direct atom-atom collisions that eject atoms, and because the openness of the crystal prevents energy randomization. It appears that the application of the transport theories to semiconductors is at best a dangerous practice. The binding energy of a Si atom in the top layer of the {110} or the {100} (2×1) face is 3.92 eV (three neighbor Si atoms) and that for a Si atom in the {100} face is 2.62 eV (two neighbor Si atoms). Since 50–75 % (Table II) of the atoms eject from the top layer, this binding energy difference at least partially accounts for the difference in peak positions shown in Fig. 2(b). Also shown in Fig. 2(b) is the energy distribution in the peak of the angular distribution from Si{110} along $\varphi=180°$. As for metals, this distribution maximizes at a value greater than the angle-integrated distribution.[6,7]

IV. CONCLUSIONS

The underlying mechanisms of atom ejection, due to keV particle bombardment for the open silicon lattice, have been examined using the molecular dynamics approach. Whereas for close-packed systems such as metals where surface channeling and blocking are important, for silicon the large open channels where atoms can move unimpeded allow other collision mechanisms to dominate the ejection process. Detailed angular distributions are calculated for the Si{110}, bulk terminated Si{100}, and dimer reconstructed Si{100} (2×1) faces. The angular distributions are strongly dependent on the crystal structure; thus, they should be an excellent means of determining surface atomic arrangements. The open crystal inhibits the energy from completely randomizing so that the energy distribution peaks at a high value compared to metallic systems. Our results are compared to those of Stansfield *et al.*[12] Both studies predict that there is significant ejection of atoms from below the first surface layer and similar angular distributions for the bulk terminated Si{100} face. The primary discrepancy between the two studies is the predicted angular distribution from the dimer reconstructed Si{100} (2×1) surface where their pattern has four peaks separated by 90° in the azimuthal direction and ours is more complex.

We have examined the moving atom approximation for reducing the computer time for the simulations. In this approximation, only the equations of motion of the atoms which have been struck are integrated. For the open Si lattice using a short-ranged Tersoff potential, we have found that the approximation reduces the computer time by about a factor of 3 while maintaining the integrity of the calculated yields, and energy and angular distributions. The moving atom approximation makes the possibility of examining radiation damage with molecular-dynamics simulation using realistic potentials feasible. Now one should be able to examine damage at a microscopic level.

ACKNOWLEDGMENTS

The financial support of The National Research Council (R.S.), the Office of Naval Research, the National Science Foundation, the IBM Program for the Support of

the Materials and Processing Sciences, and the Camille and Henry Dreyfus Foundation (B.J.G.) are gratefully acknowledged. Penn State University supplied a generous grant of computer time for this work. Conversations with D. W. Brenner, N. Winograd, R. Blumenthal, and K. Walzl were critical in developing the code and understanding the results. D. Clary sent us his manuscript prior to publication.

---

*On leave from Loughborough University, Leicestershire LE11 3TU, United Kingdom.

†Deceased.

[1]B. J. Garrison and N. Winograd, Science **216**, 805 (1982).

[2]B. J. Garrison, J. Am. Chem. Soc. **102**, 6553 (1980).

[3]N. Winograd, B. J. Garrison, and D. E. Harrison, Jr., Phys. Rev. Lett. **41**, 1120 (1978).

[4]R. A. Gibbs, S. P. Holland, K. E. Foley, B. J. Garrison, and N. Winograd, J. Chem. Phys. **76**, 684 (1982).

[5]N. Winograd, P. H. Kobrin, G. A. Schick, J. Singh, J. P. Baxter, and B. J. Garrison, Surf. Sci. Lett. **176**, L817 (1986).

[6]B. J. Garrison, C. T. Reimann, N. Winograd, and D. E. Harrison, Jr., Phys. Rev. B **36**, 3516 (1986).

[7]B. J. Garrison, N. Winograd, D. M. Deaven, C. T. Reimann, D. Y. Lo, T. A. Tombrello, D. E. Harrison, Jr., and M. H. Shapiro, Phys. Rev. B **37**, 7197 (1988).

[8]C. T. Reimann, K. Walzl, M. El-Maazawi, D. M. Deaven, B. J. Garrison, and N. Winograd, J. Chem. Phys. **89**, 2539 (1988).

[9]C. T. Reimann, M. El-Maazawi, K. Walzl, B. J. Garrison, N. Winograd, and D. M. Deaven, J. Chem. Phys. **90**, 2027 (1989).

[10]S. P. Holland, B. J. Garrison, and N. Winograd, Phys. Rev. Lett. **43**, 220 (1979).

[11]R. J. MacDonald, Phys. Lett. **29A**, 256 (1969); Radiat. Eff. **3**, 131 (1970); Philos. Mag. **21**, 519 (1970).

[12]R. A. Stansfield, K. Broomfield, and D. C. Clary, Phys. Rev. B **39**, 7680 (1989).

[13]R. Blumenthal, B. D. Weaver, and N. Winograd (unpublished).

[14]K. Walzl, M. El-Maazawi, A. Schmalz, R. Maboudian, and N. Winograd (unpublished).

[15]N. W. Ashcroft and N. D. Mermin, in *Solid State Physics* (Holt, Rinehart, and Winston, New York, 1976), p. 83.

[16]F. H. Stillinger and T. A. Weber, Phys. Rev. B **31**, 5262 (1985).

[17]R. Biswas and D. R. Hamann, Phys. Rev. Lett. **55**, 2001 (1985).

[18]J. Tersoff, Phys. Rev. Lett. **56**, 632 (1986).

[19]D. W. Brenner and B. J. Garrison, Phys. Rev. B **34**, 1304 (1986).

[20]J. Tersoff, Phys. Rev. B **37**, 6991 (1988).

[21]J. Tersoff, Phys. Rev. B **38**, 9902 (1988).

[22]M. I. Baskes, Phys. Rev. Lett. **59**, 2666 (1987).

[23]B. W. Dodson, Phys. Rev. B **35**, 2795 (1987).

[24]E. Kaxiras and K. C. Pandey, Phys. Rev. B **38**, 12 736 (1988).

[25]R. E. Schlier and H. E. Farnsworth, J. Chem. Phys. **30**, 917 (1959).

[26]D. E. Harrison, Jr., in *Critical Reviews in Solid State and Materials Sciences*, edited by J. E. Greene (CRC, Boca Raton, 1988), Vol. 14, Suppl. 1.

[27]D. E. Harrison, Jr. P. W. Kelly, B. J. Garrison, and N. Winograd, Surf. Sci. **76**, 311 (1978).

[28]P. Sigmund, Phys. Rev. **184**, 383 (1969).

[29]M. W. Thompson, Philos. Mag. **18**, 377 (1968).

[30]B. J. Garrison, N. Winograd, D. Lo, T. A. Tombrello, M. H. Shapiro, and D. E. Harrison, Jr., Surf. Sci. Lett. **180**, L129 (1987).

[31]B. J. Garrison, Nucl. Instrum. Methods **B17**, 305 (1986).

[32]R. Smith and D. E. Harrison, Jr., Comput. Phys. (to be published).

[33]D. W. Brenner and B. J. Garrison, Surf. Sci. **198**, 151 (1988).

[34]B. J. Garrison, M. T. Miller, and D. W. Brenner, Chem. Phys. Lett. **146**, 553 (1988).

[35]D. Srivastava, B. J. Garrison, and D. W. Brenner (unpublished).

[36]I. M. Torrens, *Interatomic Potentials* (Academic, New York, 1972).

[37]D. E. Harrison, Jr., J. Appl. Phys. **52**, 1499 (1981).

[38]N. Herbots, B. R. Appleton, T. S. Noggle, R. A. Zuhr, and S. J. Pennycock, Nucl. Instrum. Methods **B13**, 250 (1986).

[39]P. C. Zalm, J. Appl. Phys. **54**, 2660 (1983).

[40]D. E. Harrison, Jr. and C. B. Delaplain, J. Appl. Phys. **47**, 2252 (1976).

[41]C. Kittel, *Introduction to Solid State Physics*, 5th ed. (Wiley, New York, 1976), p. 74.